energies

MDPI

Article

Frequency Dynamics of Power Systems with Inertial Response Support from Wind Generation

Bruno Augusto Bastiani [1,*] and Ricardo Vasques de Oliveira [2,*]

[1] System Operation Division, Itaipu Binacional, Foz do Iguaçu 85856-970, Brazil
[2] Electrical Engineering Department, Federal University of Technology, Pato Branco 85503-390, Brazil
* Correspondence: bbast@itaipu.gov.br (B.A.B.); vasques@utfpr.edu.br (R.V.d.O.); Tel.: +55-46-3220-2576 (R.V.d.O.)

Abstract: Inertial response support from wind turbine generators has become a priority requirement in most grid codes to improve the frequency response and frequency stability margins of power systems. However, the interaction between MPPT and inertial controllers may significantly degrade the power system dynamics. Therefore, there is a need to comprehensively understand the electromechanical dynamics of power systems with high penetration of wind generation. In this context, this work proposes a simplified dynamic model to assess the electromechanical dynamics of modern power systems with inertial response support from wind generation. The proposed simplified model allows simple analyses of the intrinsic and extrinsic aspects of wind generation that directly affect the system frequency dynamics and the dynamics of wind turbine generators. As a secondary contribution, this work also provides a comprehensive assessment of intrinsic and extrinsic aspects of wind generation that significantly affect the electromechanical dynamics of power systems with inertial response support from wind generation.

Keywords: power system dynamics; wind generation; inertial control; system frequency response models

Citation: Bastiani, B.A.; Oliveira, R.V.d. Frequency Dynamics of Power Systems with Inertial Response Support from Wind Generation. *Energies* **2023**, *16*, 5280. https://doi.org/10.3390/en16145280

Academic Editor: Frede Blaabjerg

Received: 3 June 2023
Revised: 4 July 2023
Accepted: 8 July 2023
Published: 10 July 2023

1. Introduction

The wind generation installed capacity in the world reached 433 GW and 906 GW at the end of 2015 and 2022, respectively, which represents an increase of 209.2% in this period [1]. China and the USA are the countries with the highest wind generation installed capacity and reached 365.4 and 144.2 GW at the end of 2022, respectively. Asia, Europe, and the Americas, continents with the highest wind generation installed capacity, reached 436.8 GW, 255.5 GW, and 234.4 GW at the end of 2022, respectively [1]. An average growth of 15% per year is expected for the world installed capacity of wind generation in the period from 2022 to 2027 [1]. This large increase in the wind generation, expected for the coming years, may aggravate operational and control problems caused by wind turbine generators (WTGs) [1].

The degradation of power system frequency dynamics, caused by the penetration of wind generation (WG) and photovoltaic generation, is one of the most relevant challenges of modern power systems [2], which may lead to generator shutdown and load shedding by the frequency relays. System operators have proposed grid codes that require inertial response support from WTGs [3] in order to improve the frequency dynamics and frequency stability margins of power systems with relevant penetration of renewable generation [4,5]. Unlike primary frequency control, inertial control mainly improves the rate of change of frequency (RoCoF) and the frequency nadir [6].

Several control approaches to provide inertial response support have been proposed to satisfy the grid codes and improve the dynamics and reliability of power systems [7–9]. The inertial response support from WTGs that operate at the maximum power point (MPP) is one of the most employed approaches [10,11]. The use of a proper virtual inertia value is

essential to improve the inertial response and prevent the degradation of power system dynamics, which can lead to generator shutdown and load shedding [12]. On the other hand, the inertial response can lead WTGs to instability due to large deviations of the wind turbine speed [13].

Some works have suggested that the higher the value of the virtual inertia, the better the frequency behavior of the system [14]. However, the action of the classical MPPT control, typically used in commercial WTGs, associated with high values of virtual inertia, can significantly degrade the system frequency dynamics [15,16]. Thus, the typical electromechanical dynamics of power systems with high penetration of WG need to be comprehensively understood and evaluated to improve the inertial support provided by WTGs [4,17].

Simplified analytical formulations for the dynamic analyses of WTGs that support inertial response can be employed by wind farm and power system operators to assist the virtual inertia tuning and provide a comprehensive understanding of the impact of the inertial support on WTGs and system frequency response. Simplified system frequency response models have been proposed to assess the impact of the inertial support provided by WG on the dynamics of the power system frequency [18–20]. However, the models proposed in [18,20] do not consider the intrinsic dynamics of the WTG and, consequently, they cannot be employed to evaluate the WTG dynamics during the inertial contribution. In [21], a simplified system frequency response model is proposed to optimize the virtual inertia of WG, minimizing the second frequency dip caused by the wind turbine speed recovery. However, the model proposed in [21] does not consider the wind turbine speed dynamics and the influence of the MPPT on the system frequency dynamics.

Methodologies based on simplified models are proposed in [13,19] to determine the virtual inertia and the maximum speed deviation of the wind turbine. These methodologies determine the virtual inertia in such a way as to avoid stability loss of the WTG and to optimize the WTG inertial contribution. However, the approach proposed in [13] disregards the WTG dynamics in the formulation that describes the system frequency. Thus, such a formulation does not describe the detrimental coupling between the MPPT and inertial controllers on the system frequency response. Therefore, the formulation proposed in [13] is suitable only for power systems with low penetration of WG. Although the model proposed in [19] considers the coupling between the MPPT and inertial control, it is valid only for small perturbations, since the formulation is based on a linearized model.

Considering the drawbacks of the aforementioned models, the proposition of new simplified models is required to bridge the gaps in the dynamic assessment of power systems with high penetration of WG. In addition, the analysis of power systems with high penetration of WG requires the modeling of the electromechanical dynamics of WTGs, as addressed in [22].

In the context of tools to assess the dynamics of modern power systems, this work proposes a simplified dynamic model to evaluate the electromechanical dynamics of systems with WG providing inertial response support. The proposed simplified model can assess the intrinsic and extrinsic aspects of WG that directly affect the system frequency dynamics and the electromechanical dynamics of WTGs. Aspects such as the insertion level of WG and the type of control approach employed in the WTG can be easily evaluated with the proposed simplified model. The antagonistic interaction between the inertial and MPPT controllers, which degrades the system frequency response, can also be easily assessed by the proposed model. The simplified model is composed of four differential equations and accurately describes the electromechanical dynamics of the equivalent WTG and frequency response of power systems. As an innovative contribution over other simplified models, the proposed model considers the nonlinear characteristics of the wind turbine mechanical power and MPPT control. A comprehensive assessment of the intrinsic and extrinsic aspects of WG that significantly affect the electromechanical dynamics of power systems with inertial support from WTGs is also another relevant contribution of this work. The

carried-out analyses evaluate how the wind speed, value of virtual inertia, load variation magnitude, and WTG control mode affect the frequency dynamics of power systems.

Power systems with high penetration of renewable generation have more complex dynamics as compared with conventional power systems based on synchronous generators. Therefore, there is a need for understanding these new dynamics and their impact on power system dynamics and control. The proposed model, performed analyses, and obtained results provide a deeper and comprehensive understanding of the dynamics of power systems with inertial response support from WTGs. The proposed simplified model and the performed analyses are useful for the planning and operation of power systems with high penetration of WG [23], tuning of inertial controllers [24], and evaluation of new control approaches.

The paper is structured as follows. Section 2 addresses the typical electromechanical dynamics of type-4 WTGs operating with inertial control based on virtual synchronous generators (VSG). Section 3 presents the formulation of the proposed simplified model. The accuracy validation of the proposed model and the dynamic assessment of power systems with inertial response support from WG are presented in Section 4. Finally, Section 5 presents the conclusions about the proposed model and the performed dynamic assessment.

2. Electromechanical Dynamics of WTGs Operating with Inertial Controller

Among the different types of WTGs, the type-3 and type-4 WTGs are the dominant topology commercially used to provide inertial response support, due to their static converters and control loops that allow the implementation of inertial controllers [25]. Inertial response support may be provided by WTGs operating in the PQ control mode or Qf/Vf control mode [24,26]. In the PQ control mode, the WTG control loops regulate the active and reactive powers and in the Qf control mode the WTG control loops regulate the frequency and reactive power at the WTG output. PQ and Qf control modes are also known as grid-following control and grid-forming control, respectively [24,26]. In this section, type-4 WTG with its inertial controller operating in PQ and Qf control modes is briefly addressed, since it is not an innovative contribution of this work.

The control diagram of a type-4 WTG operating in the PQ control mode with inertial controller is shown in Figure 1 [8], where H_v is the virtual inertia constant, ω_t is the wind turbine speed, and k_{opt} is the gain of the classical MPPT employed in commercial WTGs. The virtual inertia moment may be written as a function of the inertia constant as $J_v = 2S_b H_v/\omega_b^2$, where S_b and ω_b are, respectively, the base power and base frequency of the WTG. The power reference assigned to the control loop of the WTG is generated by the MPPT and inertial controllers. The simultaneous action of these two controllers couples the wind turbine speed dynamics and system frequency dynamics. The control loops of the WTG are implemented in the *dq* reference frame using typical PI controllers [8].

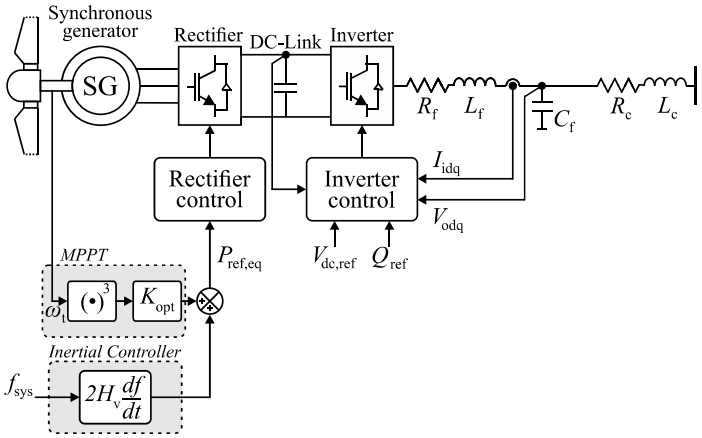

Figure 1. Typical control scheme of a type-4 wind turbine generator (WTG) in the PQ control mode.

The control diagram of a type-4 WTG operating in the Qf control mode with inertial response support from VSG is shown in Figure 2 [17]. The MPPT control generates the power reference ($P_{v,m}$) assigned to the WTG, also coupling the system frequency dynamics and wind turbine speed dynamics. The frequency (ω_v) and reactive power at the WTG output are regulated by the control loops of the inverter, which includes the VSG, and the rectifier control loop regulates the DC-link voltage [25,27]. The controllers of the inverter and rectifier are detailed addressed in [27] and [28], respectively.

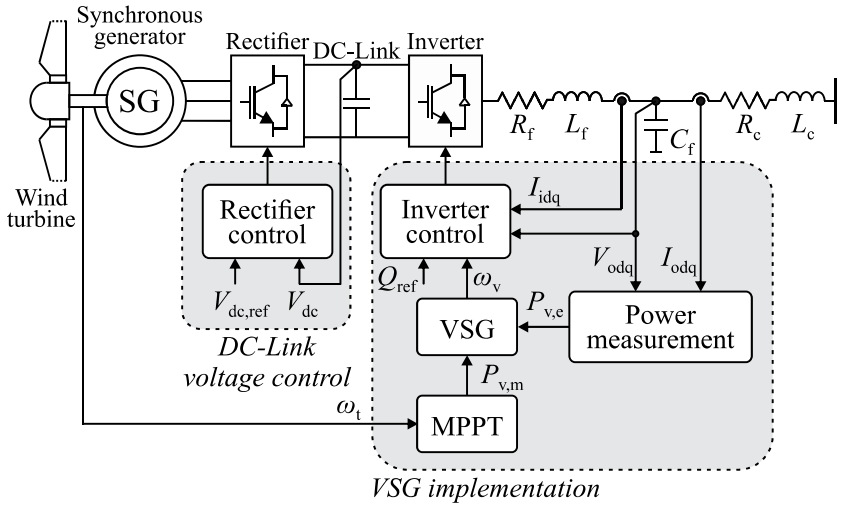

Figure 2. Typical control scheme of a type-4 WTG in the Qf control mode.

The mechanical dynamics of conventional synchronous generators, which correspond to the generator speed and inertial response, are emulated by a low-order VSG, as addressed in [24,26]. The employed VSG and MPPT are detailed in Figure 3, where ω_v is the VSG angular speed, θ_v is the virtual mechanical phase of the VSG, and D_v is the virtual damping coefficient of the VSG. The PWM algorithm of the WTG uses the angle θ_v to control the frequency at the inverter output [27,28]. A low-pass filter is employed to provide mechanical damping to the VSG [29]. In Figure 3, T_d and $\omega_{v,d}$ are the time constant and output of the low-pass filter, respectively.

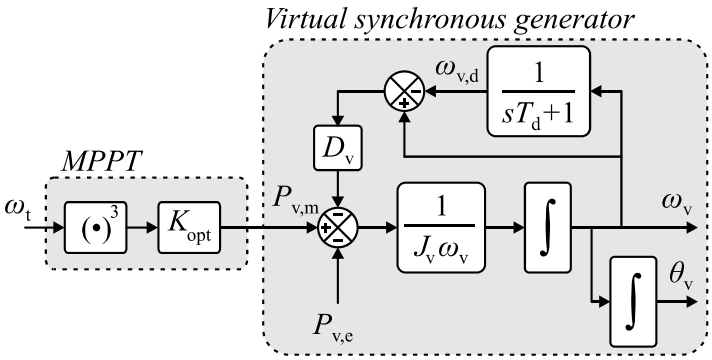

Figure 3. Model of the adopted VSG with the MPPT control.

Different kinds of generators (i.e., synchronous and asynchronous machines) are employed in commercial type-3 and type-4 WTGs. However, the different kinds of generators present the same mechanical dynamics, described by Newton's second law of motion ($J_t\omega_t d\omega_t/dt = P_{t,m} - P_{v,e}$, also presented in (4) and (A9) and known as the *swing equation*) [13,16,18,30,31]. The inertial response support of the WTGs is mainly determined by the inertial controller and its parameters [26]. Different kinds of inertial controllers are also employed in commercial WTGs, as previously addressed. However, despite the

difference between inertial controllers (i.e., grid-forming and grid-following inertial controllers), the inertial response and mechanical dynamics of the WTGs due to the inertial controller action are quite similar, as compressively assessed in [26]. In this work, the VSG control was chosen due to its grid-forming capability, which is highly desired in modern power systems. Considering that the different generators and different inertial controllers present equivalent mechanical dynamics [18,26], the proposed model can be employed to describe the mechanical dynamics of generic commercial type-3 and type-4 WTGs, if proper equivalent parameters for the generator and inertial controller are adopted.

Typical Electromechanical Dynamics

This subsection presents an analysis of the typical electromechanical dynamics of WTGs operating with inertia control. The analysis of these dynamics is relevant to show the natural coupling of the WTG dynamics and frequency dynamics, caused by the MPPT control.

The analysis assumes that at $t = t_0$ the system is subjected to a load increase, and the WTG operates at the MPP with MPPT control. The typical frequency behavior of a generic power system, which is presented in Figure 4, is commonly divided into three periods according to the dominant dynamics: (T1) inertial response, where the generators release the kinetic energy from the rotating masses; (T2) action of the primary frequency control; (T3) action of the secondary frequency control.

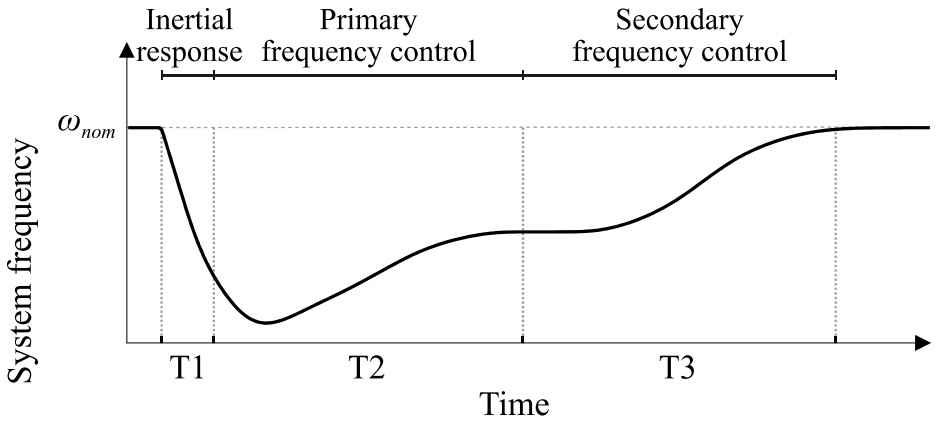

Figure 4. Typical frequency behavior of power systems.

The inertial response from the WTG is proportional to the rate of change of the frequency and, therefore, its contribution is negligible in period T3. During periods T1 and T2, the inertial controller contributes to the inertial response, releasing or absorbing energy from the system, which results in the absorption or release of kinetic energy of the wind turbine. This dynamic behavior is represented by the transient power balance of the WTG presented in Equation (1). In such a formulation, the dynamics of the DC-link voltage were neglected, since they are very fast compared to the electromechanical dynamics of the inertial controller and wind turbine.

$$\Delta P_{v,e} \cong \underbrace{\Delta P_{ref} - J_v \omega_v \frac{d\omega_v}{dt}}_{\text{Group of terms 1}} \cong \underbrace{\Delta P_{t,m} - J_t \omega_t \frac{d\omega_t}{dt}}_{\text{Group of terms 2}}. \quad (1)$$

In (1), ω_t is the wind turbine speed, ω_v is the VSG angular speed, J_v is the virtual moment of inertia of the inertial controller, J_t is the inertia moment of the wind turbine−generator set, $\Delta P_{t,m}$ is the mechanical power variation of the wind turbine, $\Delta P_{v,e}$ is the active power variation at the WTG output, and ΔP_{ref} is the variation in power reference of the VSG. In the formulations presented in this work, the variables without the upper bar are in the international system of units (SI), and the variables with the upper

bar are in the per-unit system (p.u.). The active power at the WTG output ($P_{v,e}$) during the inertial response is mainly determined by the action of the inertial and MPPT controllers. In Equation (1), the active power variation at WTG output due to the inertial controller action is given by $-J_v\omega_v\, d\omega_v/dt$, and the term $\Delta P_{ref} = K_{opt}\left(\omega_t^3 - \omega_{MPP}^3\right)$, where ω_{MPP} is the wind turbine speed at MPP, is the active power variation caused by the MPPT controller action. The wind turbine inertial power $\left(J_t\omega_t d\omega_t/dt\right)$ and the mechanical power variation of the wind turbine ($\Delta P_{t,m}$) during the inertial response are described by the group of terms 2 in Equation (1). The active power variation in the WTG ($\Delta P_{v,e}$) during the inertial response support is almost equal to the variation in the mechanical power and inertial power of the wind turbine, as shown in the transient power balance and also addressed in [17].

The transient power balance described in Equation (1) can be better understood by analyzing the wind turbine mechanical power and WTG output power illustrated in Figure 5. The dynamics of the wind turbine speed, shown in Figure 6, are also considered in this analysis. The electromechanical dynamics of the WTG are mainly affected by the inertial and MPPT controllers, as comprehensively addressed in the remainder of this section.

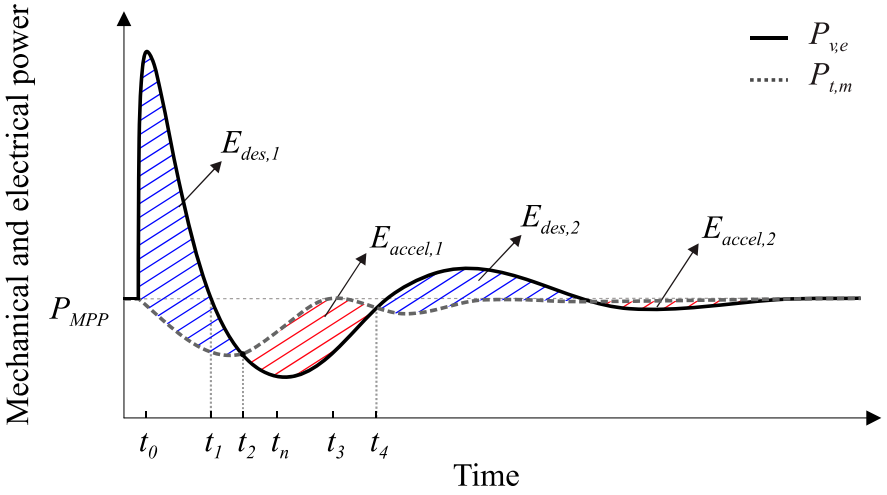

Figure 5. Typical response of the mechanical and electrical power of a WTG providing inertial response with the MPPT control active.

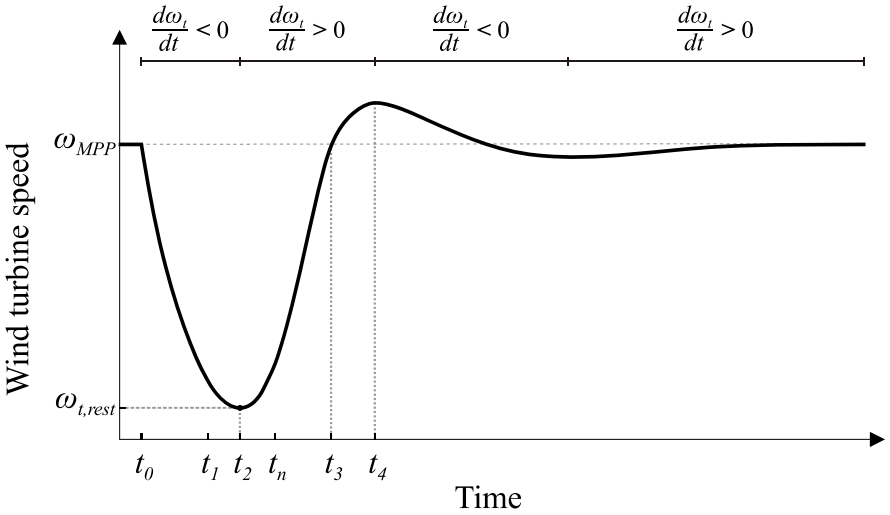

Figure 6. Typical response of the wind turbine speed of a WTG providing inertial response with MPPT control active.

After a load variation, the inertial control increases the active power supplied by the WTG, resulting in a positive power variation ($\Delta P_{v,e}$). A positive $\Delta P_{v,e}$ provides decelerating energy ($E_{des,1}$) to the wind turbine, resulting in the turbine deceleration and negative variation of the turbine mechanical power ($\Delta P_{t,m}$). The decelerating energy provided to the wind turbine is equal to the kinetic energy variation of the wind turbine (ΔE_k), which corresponds to the area between $P_{v,e}$ and $P_{t,m}$, illustrated in Figure 5.

Analyzing Equation (1) and Figures 5 and 6, it is possible to observe that the inertial power ($J_t \omega_t d\omega_t / dt$) and $\Delta P_{t,m}$ are negative in the period between t_0 and t_2. Thus, considering that $\Delta P_{v,e} = \Delta P_{t,m} - J_t \omega_t d\omega_t / dt$, as showed in Equation (1), it is possible to conclude that only part of the wind turbine inertial power is delivered to the grid by the inertia controller. It is worth remarking that this analysis is valid for MPPT operation, since in de-loaded operation in the over-speed region, a wind turbine deceleration increases the mechanical power ($\Delta P_{t,m} > 0$). The increase of $P_{t,m}$, in the de-loaded operation, increases the power delivered to the grid ($P_{v,e}$) by the inertial controller.

The MPPT control also affects the inertial response support of the WTG. As the wind turbine slows down, the MPPT control reduces the power reference of the WTG (ΔP_{ref}), reducing $\Delta P_{v,e}$ to accelerate the wind turbine towards the MPP speed. During the wind turbine speed recovery, the MPPT and inertial controllers have antagonistic actions. The detrimental interaction of the MPPT reduces the inertial response support of the WTG, which is equivalent to reducing the virtual inertia (J_v) assigned to the inertial controller.

Besides reducing the inertial response support of the WTGs, the MPPT control makes $\Delta P_{v,e}$ negative before the occurrence of the frequency nadir (t_n). The decrease of $P_{v,e}$, which can be observed in Figure 5, after t_1, reduces the frequency nadir, degrading the system frequency response. The wind turbine deceleration ceases when $P_{v,e}$ becomes equal to $P_{t,m}$, at time t_2.

The output power $P_{v,e}$ becomes smaller than $P_{t,m}$ after t_2, providing accelerating energy ($E_{accel,1}$) to the wind turbine. After time t_n, the RoCoF becomes positive and, consequently, the inertial controller reduces the magnitude of $P_{v,e}$. Thus, the MPPT and inertial controllers accelerate the wind turbine towards the MPP, as shown in Figure 6. This synergetic action of both controllers leads to an overshoot in the wind turbine speed ($\omega_t > \omega_{MPP}$). After ω_t becomes higher than ω_{MPP} ($\Delta\omega_t > 0$), the MPPT acts to decelerate the turbine, increasing $P_{v,e}$, while the inertial control reduces $P_{v,e}$, accelerating the wind turbine. This antagonistic action of the MPPT and inertial controllers lasts until time t_4, when $P_{v,e}$ becomes equal to $P_{t,m}$ again. The performed analysis shows that the interaction of the MPPT and inertial controllers alternates between synergetic and antagonistic actions during the dynamics of the system frequency. Such alternance supply accelerating and decelerating energy to the wind turbine (E_{des} and E_{accel}), leading to an oscillatory response to the wind turbine speed and output power of the WTG.

It is worth remarking that the WTG would naturally oscillate around the MPP only due to the MPPT control action. However, the interaction between the MPPT and inertial controllers increases the oscillation of the output power and wind turbine speed. The results presented in Section 4 show that the amplitude of these oscillations varies as a function of the load variation magnitude, virtual inertial of the VSG, and WTG operating point.

Based on the term $P_{v,e} \cong K_{opt}\left(\omega_t^3 - \omega_{MPP}^3\right) - J_v \omega_v d\omega_v / dt$ presented in Equation (1), it is possible to characterize the antagonistic or synergetic interaction of the inertia and MPPT controllers as a function of the speed deviation of the wind turbine ($\Delta\omega_t = \omega_t - \omega_{MPP}$) and system frequency derivative ($d\omega_v / dt$). The Cartesian space $d\omega_v / dt$ versus $\Delta\omega_t$, illustrated in Figure 7, characterizes the antagonistic and synergetic interactions of the MPPT and inertial controllers. As previously addressed, the antagonistic interaction reduces the effectiveness of the inertial support provided by the inertial control, and the synergetic interaction increases the system oscillations.

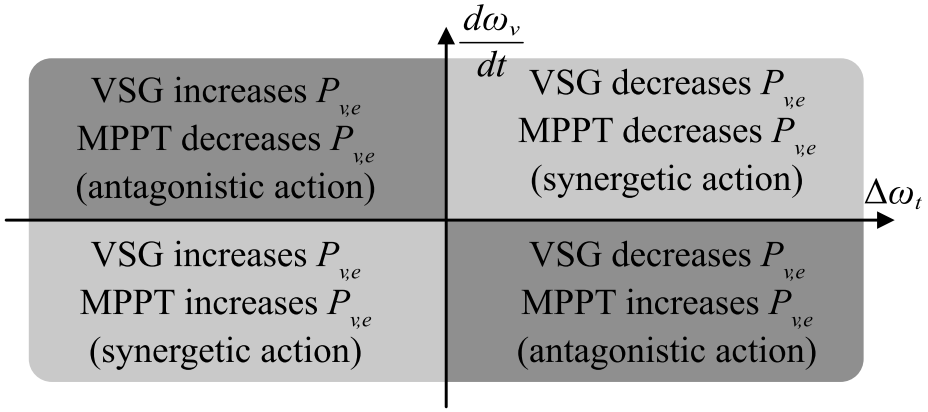

Figure 7. Impact of the VSG and MPPT on the WTG output power.

3. Simplified Model Proposed to Assess the Electromechanical Dynamics

The formulation of the simplified model proposed to assess the electromechanical dynamics of modern power systems with WG providing inertial response is addressed in this section. The proposed model describes the electromechanical dynamics of large generic equivalent power systems, composed of an equivalent WTG, representing a set of wind farms, an equivalent synchronous generator, representing the set of conventional synchronous generators, and an equivalent load.

The simplified model is composed of four nonlinear differential equations. Simplifying hypotheses are adopted to provide a low-order model that accurately describes the dynamics of power systems. The adopted simplifying assumptions are typically employed in dynamic analyses of power systems. Dynamics significantly faster than the system frequency dynamics are disregarded, since they do not significantly affect the dynamics of interest [29]. The switching dynamics of the WTG static converter, the DC link dynamics of the WTG, the LCL filter dynamics of the WTG, and the damping component of the VSG are neglected.

The mechanical dynamics of the equivalent synchronous generator and equivalent WTG, considering the previously mentioned assumptions, are described by [29]:

$$\frac{J_{sg}\omega_{base}^2}{S_{sg,base}}\overline{\omega}_{sg}\frac{d\overline{\omega}_{sg}}{dt} = \Delta\overline{P}_{sg,m} - \Delta\overline{P}_{sg,e}, \tag{2}$$

$$\frac{J_{v}\omega_{base}^2}{S_{t,base}}\overline{\omega}_{v}\frac{d\overline{\omega}_{v}}{dt} = \Delta\overline{P}_{v,m} - \Delta\overline{P}_{v,e}, \tag{3}$$

$$\frac{J_{t}\omega_{t,base}^2}{S_{t,base}}\overline{\omega}_{t}\frac{d\overline{\omega}_{t}}{dt} = \Delta\overline{P}_{t,m} - \Delta\overline{P}_{v,e}, \tag{4}$$

where $\overline{\omega}_{sg}$ and $\overline{\omega}_{v}$ are, respectively, the angular frequencies of the equivalent synchronous generator and equivalent WTG, J_{sg} and J_v are the inertia moments of the equivalent synchronous generator and equivalent WTG, respectively, $\Delta\overline{P}_{sg,m}$ and $\Delta\overline{P}_{v,m}$ are, respectively, the mechanical power of the equivalent synchronous generator and virtual mechanical power of the WTG, $\Delta\overline{P}_{sg,e}$ and $\Delta\overline{P}_{v,e}$ are the output power of the equivalent synchronous generator and equivalent WTG, respectively, $\overline{\omega}_t$ is the wind turbine speed, J_t is the inertia moment of the equivalent wind turbine, $\Delta\overline{P}_{t,m}$ is the mechanical power of the wind turbine, ω_{base} and $\omega_{t,base}$ are, respectively, the base frequencies of the system and wind turbine, and $S_{sg,base}$ and $S_{t,base}$ are the base powers of the equivalent synchronous generator and equivalent WTG, respectively.

Equation (2) is represented on the base power of the equivalent synchronous generator and Equations (3) and (4) are on the base power of the equivalent WTG. Therefore, Equations (2)–(4) are rewritten in the base power of the power system ($S_{sys,base}$) as:

$$\frac{J_{sg}\omega_{base}^2}{S_{sg,base}}\overline{\omega}_{sg}\frac{d\overline{\omega}_{sg}}{dt}\frac{S_{sg,base}}{S_{sys,base}} = \Delta\overline{P}_{sg,m} - \Delta\overline{P}_{sg,e}, \tag{5}$$

$$\frac{J_{v}\omega_{base}^2}{S_{t,base}}\overline{\omega}_{v}\frac{d\overline{\omega}_{v}}{dt}\frac{S_{t,base}}{S_{sys,base}} = \Delta\overline{P}_{v,m} - \Delta\overline{P}_{v,e}, \tag{6}$$

$$\frac{J_{t}\omega_{t,base}^2}{S_{t,base}}\overline{\omega}_{t}\frac{d\overline{\omega}_{t}}{dt}\frac{S_{t,base}}{S_{sys,base}} = \Delta\overline{P}_{t,m} - \Delta\overline{P}_{v,e}. \tag{7}$$

The relation $d_w = S_{t,base}/S_{sys,base}$ is the index of replacement of conventional generation by WG, also known as the WG penetration level. Considering that the base power of the system is given by:

$$S_{sys,base} = S_{t,base} + S_{sg,base}. \tag{8}$$

The term $S_{sg,base}/S_{sys,base}$, in Equation (5), can also be written as a function of d_w, as:

$$1 - d_w = \frac{S_{sg,base}}{S_{sys,base}}. \tag{9}$$

Using the index d_w and replacing the inertia moment J_{sg} and J_v by the inertia constant H_{sg} and H_v, the model (5)–(7) is rewritten as:

$$2H_{sg}(1 - d_w)\overline{\omega}_{sg}\frac{d\overline{\omega}_{sg}}{dt} = \Delta\overline{P}_{sg,m} - \Delta\overline{P}_{sg,e}, \tag{10}$$

$$d_w 2H_{v}\overline{\omega}_{v}\frac{d\overline{\omega}_{v}}{dt} = \Delta\overline{P}_{v,m} - \Delta\overline{P}_{v,e}, \tag{11}$$

$$d_w J_t\frac{\omega_{t,base}^2}{S_{t,base}}\overline{\omega}_{t}\frac{d\overline{\omega}_{t}}{dt} = \Delta\overline{P}_{t,m} - \Delta\overline{P}_{v,e}. \tag{12}$$

The frequencies $\overline{\omega}_{sg}$ and $\overline{\omega}_{v}$, during the dominant inertial response (i.e., period T1 in Figure 4), may present slightly different instantaneous values. However, the mean value of these frequencies over a time window of about hundreds of *ms* can be considered equal in analyses of system frequency dynamics. Thus, considering $\overline{\omega}_{sg} = \overline{\omega}_{v} = \overline{\omega}$, Equations (10) and (11) can be rewritten as:

$$2H_{sg}(1 - d_w)\overline{\omega}\frac{d\overline{\omega}}{dt} = \Delta\overline{P}_{sg,m} - \Delta\overline{P}_{sg,e}, \tag{13}$$

$$d_w 2H_{v}\overline{\omega}\frac{d\overline{\omega}}{dt} = \Delta\overline{P}_{v,m} - \Delta\overline{P}_{v,e}. \tag{14}$$

Isolating the term $d\overline{\omega}/dt$ in Equation (13) and replacing in Equation (14), results in Equation (15).

$$\frac{\Delta\overline{P}_{v,m} - \Delta\overline{P}_{v,e}}{d_w 2H_v} = \frac{\Delta\overline{P}_{sg,m} - \Delta\overline{P}_{sg,e}}{2H_{sg}(1 - d_w)}. \tag{15}$$

Considering the system load variation $\Delta\overline{P}_L$, given by Equation (16), it is possible to isolate the term $\Delta\overline{P}_{sg,e}$ and replace it in Equation (15), which results in Equation (17).

$$\Delta\overline{P}_L = \Delta\overline{P}_{sg,e} + \Delta\overline{P}_{v,e}. \tag{16}$$

$$\frac{\Delta\overline{P}_{v,m} - \Delta\overline{P}_{v,e}}{d_w 2H_v} = \frac{\Delta\overline{P}_{sg,m} - \left(\Delta\overline{P}_L - \Delta\overline{P}_{v,e}\right)}{2H_{sg}(1-d_w)}. \tag{17}$$

The output power of the equivalent WTG can be written from Equation (17) as:

$$\Delta\overline{P}_{v,e} = \frac{2H_{sg}(1-d_w)\Delta\overline{P}_{v,m} + 2H_v d_w\left(\Delta\overline{P}_{sg,m} - \Delta\overline{P}_L\right)}{\left(2H_{sg}(1-d_w) + 2H_v d_w\right)}. \tag{18}$$

Replacing Equation (18) in Equation (12), it is possible to describe the dynamics of the wind turbine speed as:

$$d_w J_t \frac{\omega_{t,base}^2}{S_{t,base}} \overline{\omega}_t \frac{d\overline{\omega}_t}{dt} = \Delta\overline{P}_{t,m} + \frac{2H_v d_w\left(\Delta\overline{P}_{sg,m} - \Delta\overline{P}_L\right) - 2H_{sg}(1-d_w)\Delta\overline{P}_{v,m}}{\left(2H_{sg}(1-d_w) + 2H_v d_w\right)}. \tag{19}$$

The system frequency dynamics can be obtained by isolating $\Delta\overline{P}_{sg,e}$ in Equation (13) and $\Delta\overline{P}_{v,e}$ in Equation (14), and replacing both equations in Equation (16), which results in:

$$\left(2H_{sg}(1-d_w) + 2H_v d_w\right)\overline{\omega}\frac{d\overline{\omega}}{dt} = \Delta\overline{P}_{sg,m} + \Delta\overline{P}_{v,m} - \left(\Delta\overline{P}_{sg,e} + \Delta\overline{P}_{v,e}\right). \tag{20}$$

The term $\left(\Delta\overline{P}_{sg,e} + \Delta\overline{P}_{v,e}\right)$ in Equation (20) can be replaced by $\Delta\overline{P}_L$, presented in Equation (16), which results in Equation (21). It is possible to observe in Equation (21) that the system frequency dynamics depend on $\Delta\overline{P}_{v,m}$, which represents the power reference provided by the MPPT control as a function of wind turbine speed ($\overline{P}_{v,m} = k_{opt}\overline{\omega}_t^3$). This aspect consistently shows a coupling between the dynamics of the wind turbine speed and the system frequency. Therefore, the degradation of the inertial response, caused by such coupling, can be assessed using the proposed model.

$$\left(2H_{sg}(1-d_w) + 2H_v d_w\right)\overline{\omega}\frac{d\overline{\omega}}{dt} = \Delta\overline{P}_{sg,m} + \Delta\overline{P}_{v,m} - \Delta\overline{P}_L. \tag{21}$$

The proposed model can represent different kinds of conventional generation units, such as steam units and hydraulic units, different kinds of MPPT control, and different de-loaded approaches for the WTG. These control approaches are related to the power variation $\Delta\overline{P}_{sg,m}$ and $\Delta\overline{P}_{v,m.}$ Considering the conventional MPPT control for the WTG, the power variation $\Delta\overline{P}_{v,m}$ is given by:

$$\Delta\overline{P}_{v,m} = k_{opt}\left(\overline{\omega}_t^3 - \overline{\omega}_{MPP}^3\right), \tag{22}$$

where k_{opt} is the optimal gain of the MPPT control and $\overline{\omega}_{MPP}$ is the wind turbine speed at MPP. The conventional generation considered in this work is a steam unit, whose mechanical power is described by the simplified model (23) and (24) [30].

$$\frac{d\overline{x}}{dt} = \frac{1}{T_{CH}}(\Delta u - \overline{x}), \tag{23}$$

$$\frac{d\Delta\overline{P}_{sg,m}}{dt} = \frac{1}{T_{CH}}\left(\overline{x} - \Delta\overline{P}_{sg,m} - F_{HP}T_{RH}\frac{d\overline{x}}{dt}\right). \tag{24}$$

In Equations (23) and (24), Δu is the control signal corresponding to the primary frequency control of the synchronous generator, T_{CH} is the reheater time constant, F_{HP} is the fraction of total power generated by the turbine high-pressure section, and $\overline{x}$ is an auxiliary variable. The secondary frequency control was not considered in the proposed study since its impact is negligible on the dynamics of the inertial control and primary frequency control.

The set of nonlinear differential Equations (19), (21), (23) and (24) composes the final simplified model, which describes the system frequency dynamics and dynamics of the equivalent WTG providing inertial response support. This proposed model can be used in different contexts to assess the impact of WG integration on the system frequency dynamics. The model also allows the inclusion of the primary frequency control in WG. However, this work is focused only on the inertial response support.

The mechanical power deviation of the wind turbine, employed in Equation (19), is given by

$$\Delta\overline{P}_{t,m} = \overline{P}_{t,m} - \overline{P}_{t,m,MPP}. \tag{25}$$

The mechanical power $\overline{P}_{t,m}$ is given by the wind turbine aerodynamic model, presented in the Appendix A, and $\overline{P}_{t,m,MPP}$ is the mechanical power at the MPP (i.e., $\overline{P}_{t,m,MPP|_{\overline{\omega}_{MPP}}}$).

Algorithm 1 describes the steps to perform dynamic analyses with the proposed model. The wind turbine speed ($\overline{\omega}_t$), system frequency ($\overline{\omega} = \overline{f}$), and mechanical power of the synchronous equivalent generator ($\Delta\overline{P}_{sg,m}$) are the state variables of the model. The output power of the equivalent WTG ($\Delta\overline{P}_{v,e}$), wind turbine mechanical power ($\Delta\overline{P}_{t,m}$), and mechanical power of the VSG ($\Delta\overline{P}_{v,m}$), also variables of the model, are determined by Equations (18), (22) and (25). The wind speed, V_w, and systema load variation, $\Delta\overline{P}_L$, are the input variables of the model. The virtual inertia, H_v, and the penetration index of WG, d_w, are the main parameters assigned to the WG. The proposed model can also be represented in the form of block diagram, as illustrated in Figure 8. The antagonistic action of the MPPT ($\Delta\overline{P}_{v,m}$) and inertial controllers, which affects the output power of the WTG, $\Delta\overline{P}_{v,e}$, is more evident in such block diagram.

Algorithm 1: Dynamic analyses with the proposed model

1. Chose the desired virtual inertia for the WG, H_v, and the penetration index of WG, d_w.
2. Chose the wind speed of interest, V_w, and the magnitude of the system load variation, $\Delta\overline{P}_L$.
3. Chose the parameters of the equivalent synchronous generator and equivalent WTG (i.e., wind turbine parameters in (A1)–(A4) presented in the Appendix A).
4. Calculate the initial operating point of the equivalent WTG, $\overline{\omega}_t(0) = \overline{\omega}_{MPP}$ and $\overline{P}_{t,m}(0) = \overline{P}_{t,m,MPP}$.
5. Solve Equations (19), (21), (23) and (24) using any generic differential equation solver.
6. Assess the system dynamics by means of the state variables and variables $\Delta\overline{P}_{v,e}$, $\Delta\overline{P}_{v,m}$, and $\Delta\overline{P}_{t,m}$.

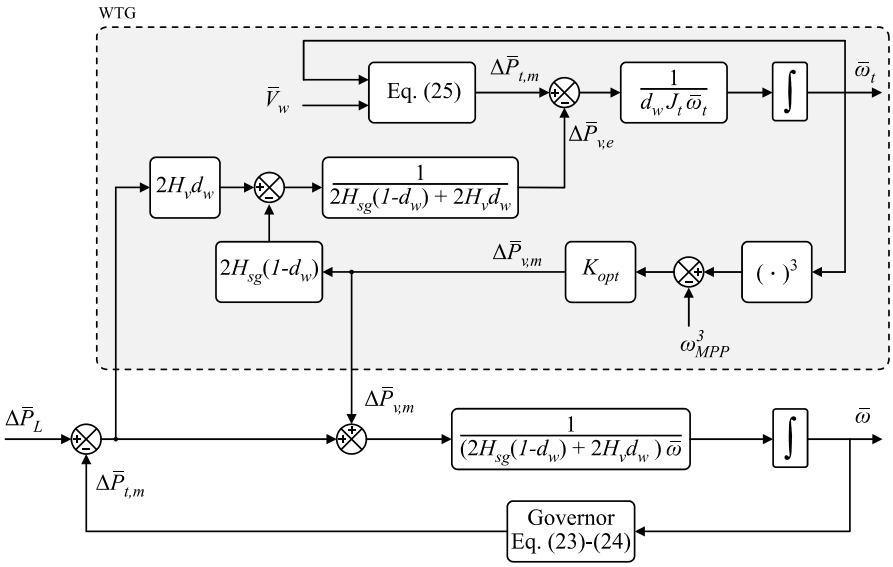

Figure 8. Block diagram of the proposed model.

The MPPT control, nonlinearity of the mechanical power curve of the wind turbine, and virtual inertia are the main intrinsic aspects of WG that affect the dynamics of WTGs and power system frequency. The wind speed and load variation magnitude are extrinsic aspects that also affect the system frequency dynamics. The additional power provided by the inertial control is almost proportional to the virtual inertia and magnitude of the load variation. However, the detrimental impact of the MPPT control is nonlinear as a function of the wind turbine speed deviation. There is also a nonlinearity in the mechanical power of the wind turbine as a function of the wind speed. The nonlinearities of the wind turbine mechanical power and MPPT control action affect the frequency dynamics of power systems. These practical aspects are addressed in the practical analyses presented in the next section.

It is worth remarking that the performed analyses are also valid for type-3 WTG with VSG, since the wind turbines of type-3 and type-4 WTGs with inertial control have similar mechanical dynamics [18,26], as addressed in Section 2.

4. Results and Discussions

The effectiveness and accuracy of the proposed model and the system dynamics are evaluated with nonlinear time-domain simulations. Initially, the performed analyses compare a high-order model of the test system with the simplified proposed model to validate the proposed model. In the sequence, the proposed model is employed to comprehensively assess the typical electromechanical dynamics of power systems with high penetration level of WG with inertial response support. These analyses consider different aspects that affect the system dynamics, such as wind speed, virtual inertia value, control mode of the WTG, and load variation magnitude.

The employed test system is composed of one equivalent wind farm (WF) and one equivalent steam generation unit with a conventional synchronous generator (SG), as shown in Figure 9. Both generation units have nominal power of 900 MVA in the base scenario, which results in a WG penetration of 50%.

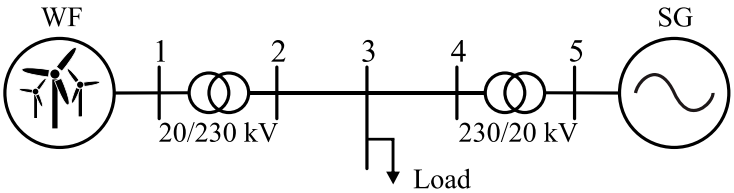

Figure 9. Topology of the employed test system.

The equivalent test system, inspired by the Kundur test system [30], highlights the dynamics of multiple WFs operating simultaneously and the impact of the MPPT and inertial control on the system frequency dynamics of bulk power systems. The equivalent SG represents the system multiple generators, as typically considered in frequency dynamics studies [20]. WFs, composed of multiple WTGs operating in parallel, are typically represented by equivalent models in frequency regulation studies [32]. Such equivalent models can accurately describe the mechanical dynamics and system frequency dynamics [32]. The computational effort and modeling complexity inherent to dynamic analyses can be considerably reduced with the use of accurate equivalent models of WFs [33]. An equivalent model, for example, is employed in [17] to represent a 900 MW WF in a dynamic analysis of a bulk power system.

A 47th-order model of the test system is employed in the performed analyses only to validate the proposed simplified model. The high-order model has also been used in the dynamic assessment presented in [22] and it is concisely described in the Appendix A. Such a model was implemented in the *dq* reference frame [34] and describes with high accuracy the electromechanical dynamics of the equivalent WTG and SG, as compared with the classical linear models employed in frequency studies of bulk power systems [18].

The system model, represented by ordinary differential equations, was implemented in the Matlab® software (version 9.13) using programming code. The *ODE23tb* solver was employed in the programming interface of the Matlab® to perform the time-domain simulations.

4.1. Accuracy Validation of the Proposed Simplified Model

The accuracy of the proposed simplified model is evaluated in this section considering the 47th-order model previously mentioned. The nonlinear simulations consider the occurrence of a load step in the test system at t = 1 s. The WF operates with H_v = 10 p.u.s and wind speed of 9 m/s, which results in an MPP speed of 0.9 p.u. and active power of 0.154 p.u. in the system base power. The equivalent conventional generator operates with an initial active power of 0.2 p.u. and H_{sg} = 5.6 p.u.s. The simplified model is evaluated in two scenarios: (1) small load variation of 1%; (2) large load variation of 3%.

Figure 10 presents the electromechanical dynamics of the test system considering the simplified model and the 47th-order model for scenarios 1 and 2. As illustrated in Figure 10a, the simplified model describes the system frequency with high accuracy in the two scenarios. The same high accuracy is observed in the wind turbine speed shown in Figure 10b. The output power of the equivalent WTG ($\overline{P}_{v,e}$), shown in Figure 10c, presents a relevant error during the first 3 s of the dynamic response. Such an error occurs because the simplified model does not represent the electromagnetic dynamics of the WTG, since the model is predominantly composed of mechanical equations. Thus, the proposed simplified model is not suitable to access electromagnetic dynamics of WTGs.

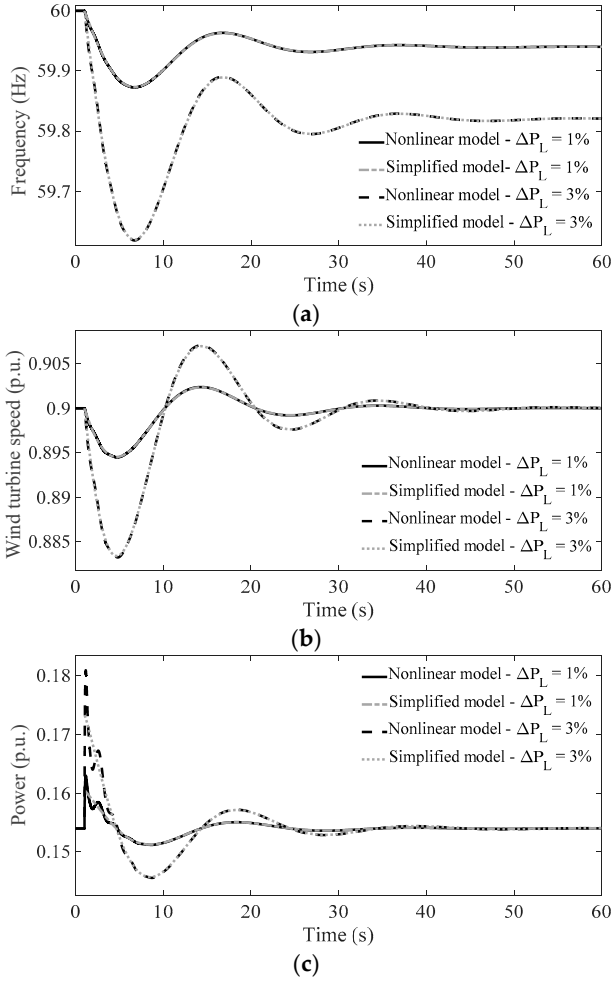

Figure 10. Accuracy assessment of the proposed simplified model for two different load variations. (**a**) Frequency of the system. (**b**) Wind turbine speed. (**c**) WTG output power.

4.2. Impact of the Inertial Controller on the Frequency Nadir and Frequency Oscillations

The inertial controller of the WG changes the dynamic behavior of the system frequency, affecting the RoCoF and frequency nadir. In addition, the simultaneous action of the inertial and MPPT controllers causes frequency oscillations that may result in a relevant second frequency dip after load variations. Such a phenomenon is comprehensively evaluated in this section, based on the analysis of the system frequency dynamics and dynamics of the equivalent WTG. The analysis is performed with the proposed simplified model considering different wind speeds and virtual inertia values.

Figure 11a shows the system frequency dynamics for a wind speed of 9 m/s and virtual inertias of 5, 10, and 15 p.u.s for the equivalent WTG. The conventional generator operates with an initial active power of 0.2 p.u. and H_{sg} = 5.6 p.u.s. This analysis shows that, unlike the behavior of conventional generation, the significant increase in the virtual inertia resulted in a negligible improvement of the frequency nadir and a considerable increase in the amplitude of the frequency oscillations.

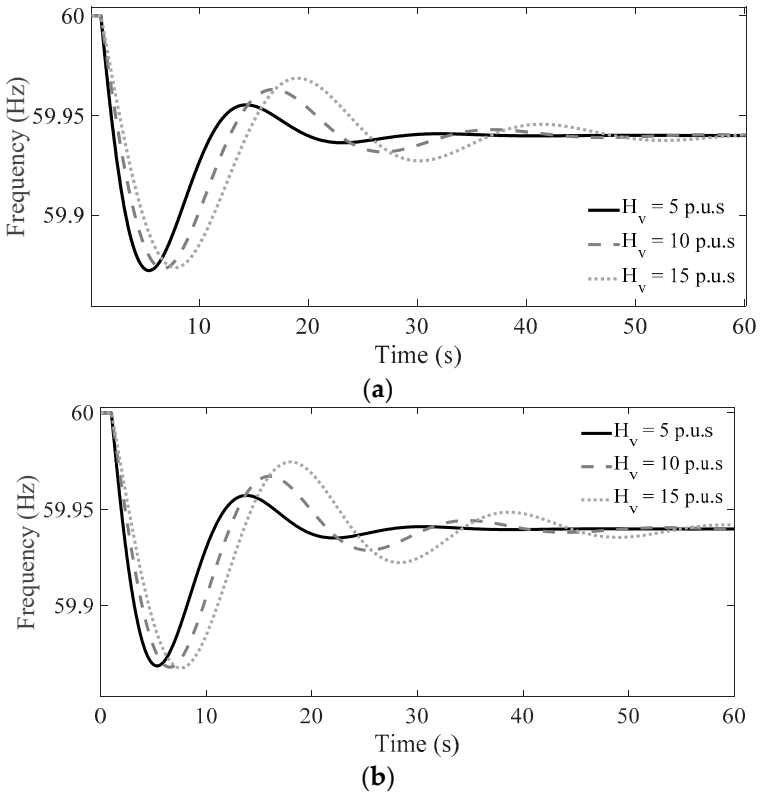

Figure 11. System frequency dynamics for different values of virtual inertia and wind speed. (**a**) System frequency for a wind speed of 9 m/s. (**b**) System frequency for a wind speed of 12 m/s.

Figure 11b shows the system frequency dynamics for the wind speed of 12 m/s and virtual inertias of 5 p.u.s, 10 p.u.s, and 15 p.u.s. It is possible to observe that the increase in the virtual inertia of the WG also causes an increase in the amplitude of the frequency oscillations. However, unlike the results presented in Figure 11a, the frequency nadir slightly decreases with the increase of the virtual inertia. The increase in the inertia in the conventional synchronous generation improves the frequency nadir, while the increase in the virtual inertia of the WG has degraded the frequency nadir. This detrimental dynamic behavior is caused by the nonlinearity of the mechanical power curve of the wind turbine ($\overline{P}_{t,m}$) and the action of the MPPT controller ($\Delta\overline{P}_{v,m} = k_{opt}\overline{\omega}_t^3$). The powers $\overline{P}_{t,m}$ and $\overline{P}_{v,m}$ present higher variation for higher wind speed. As shown in Equation (21), $\Delta\overline{P}_{t,m}$ and $\Delta\overline{P}_{v,m}$ affect the system frequency dynamics and degrade the frequency nadir.

The increase in the frequency oscillations is caused by the increase in the inertial contribution of the equivalent WTG, as can be seen in the wind turbine speed and WTG output power shown in Figure 12. As shown in Figure 12a, the higher the inertial contribution, the higher the wind turbine speed deviation and MPPT control action ($\Delta\overline{P}_{v,m} = k_{opt}(\overline{\omega}_t^3 - \overline{\omega}_{MPP}^3)$). The MPPT control action reduces the WTG output power to restore the wind turbine speed, which reduces the minimum output power, as can be observed in Figure 12b.

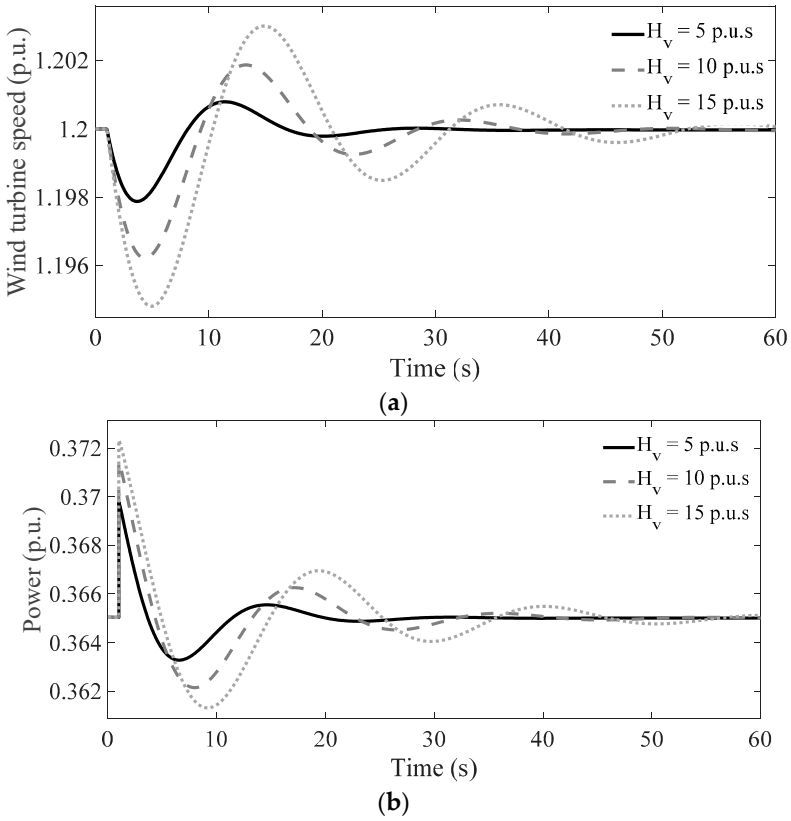

Figure 12. Dynamics of the equivalent WTG for different virtual inertia values and a wind speed of 12 m/s. (**a**) Wind turbine speed. (**b**) Output power of the WTG.

The MPPT control action starts to accelerate the wind turbine towards the MPP speed at t = 4.35 s, before the frequency nadir, which occurs at t = 6.55 s for H_v = 10 p.u.s and V_w = 12 m/s. Up to the frequency nadir, at t = 6.55 s, the inertial and the MPPT controllers have antagonistic actions, where the inertial controller provides decelerating energy to the wind turbine and the MPPT controller provides accelerating energy. However, during the positive rate of change of the system frequency, after t = 6.55 s, both controllers present synergetic actions, accelerating simultaneously the wind turbine, which causes an overshoot in the wind turbine speed. The higher the virtual inertia, the higher the overshoot of the wind turbine speed. This overshoot results in oscillations in the wind turbine speed and, due to the coupling between the wind turbine speed and system frequency, such oscillations propagate to the system frequency.

Figure 13 shows the system frequency nadir as a function of wind speed and virtual inertia. The increase in the virtual inertia increases the frequency nadir for wind speeds below 10.4 m/s and reduces the frequency nadir for wind speeds above 10.4 m/s. Such behavior is caused by the nonlinearities of the wind turbine mechanical power as a function of the wind speed. Although there is an increase in the frequency nadir for some operational conditions, this increase is not significant. As the characteristic of the wind turbine mechanical power ($\overline{P}_{t,m}$) plays an essential role in this behavior, different mechanical models of wind turbines may result in different behaviors. The wind turbine

model presented in [35], which is different from the model adopted in this work [36], for example, does not increase the frequency nadir with the increase of the virtual inertia over the entire operational range of the wind turbine.

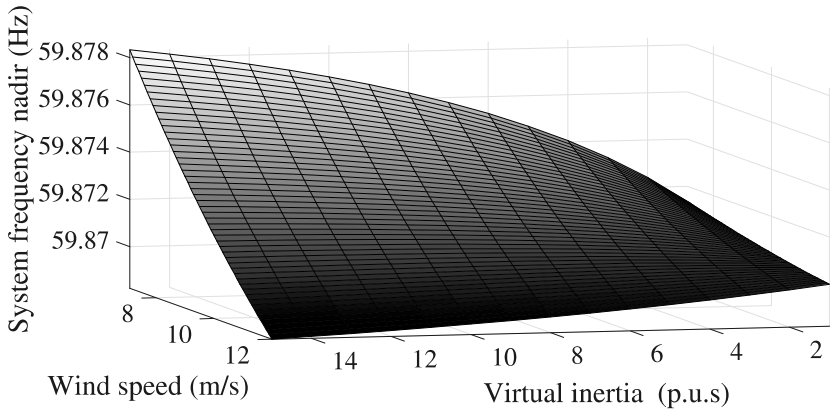

Figure 13. Frequency nadir as a function of the virtual inertia and wind speed.

4.3. Impact of the Control Mode of the WG on the System Dynamics

The impact of the WG control mode on the system frequency dynamics is evaluated in this section considering different control modes. Three control modes typically employed in commercial WTG are evaluated: (1) MPPT control; (2) de-loaded control with de-loaded power curve; (3) de-loaded control with fixed power reference. The equivalent WTG operates with H_v = 10 p.u.s and a wind speed of 9 m/s in the three scenarios.

The de-loaded operation with a de-loaded power curve is based on Equation (22), where the optimal gain is replaced by a sub-optimal gain as a function of a desired de-loading factor [37]. On the other hand, the de-loaded operation with a fixed power reference uses a constant power reference for the WTG (i.e., $\overline{P}_{v,m} = \overline{P}_{ref,const}$, which implies that $\Delta\overline{P}_{v,m} = 0$). This fixed power reference for the WTG, also employed in [17], decouples the wind turbine speed dynamics from the system frequency dynamics. A high de-loaded margin of 50% has been employed to highlight the difference between the dynamics of the MPPT and de-loaded control modes.

Figure 14 presents the system frequency for the three control modes, where scenarios 1, 2, and 3 resulted in frequency nadirs of 59.873 Hz, 59.882 Hz, and 59.898 Hz, respectively. The improvement of the frequency nadir in scenario 2 occurs because the MPPT gain (k_{opt}) is reduced to provide a de-loaded margin, reducing the amplitude of the coupling term $\Delta\overline{P}_{v,m}$ in Equation (21). In scenario 3, the frequency nadir improvement occurs due to the decoupling between the dynamics of the wind turbine speed and system frequency, caused by $\Delta\overline{P}_{v,m} = 0$.

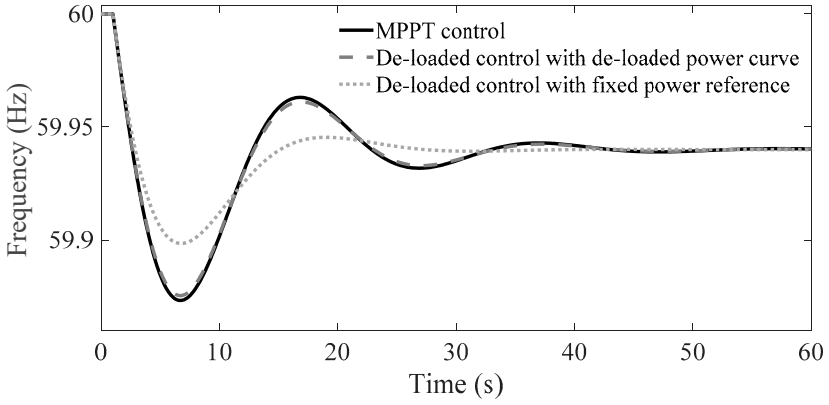

Figure 14. System frequency for three control modes typically employed in commercial WTGs.

4.4. Impact of the WG Penetration Level on System Dynamics

The analysis presented in this subsection comprehensively shows the impact of the WG penetration level on the dynamics of the system frequency and equivalent WTG. WG penetrations of 20%, 40%, and 60% are considered in the analysis. The three scenarios consider wind speed of 9 m/s and virtual inertia of 10 p.u.s for the equivalent WTG operating with classical MPPT control.

The increase in the WG penetration level has significantly degraded the frequency nadir, steady-state frequency error, and electromechanical oscillations, as shown in Figure 15a. The reduction in the frequency nadir and the increase in the steady-state frequency error occur due to the absence of primary frequency control in the WG. The oscillations have been caused by the interaction between the MPPT and inertial controllers. Therefore, inertial control is necessary but not sufficient to provide a suitable performance to the system. The minimum speed of the wind turbine, shown in Figure 15b, reduces with the increase of the WG insertion level due to the increase in the frequency dip of the system.

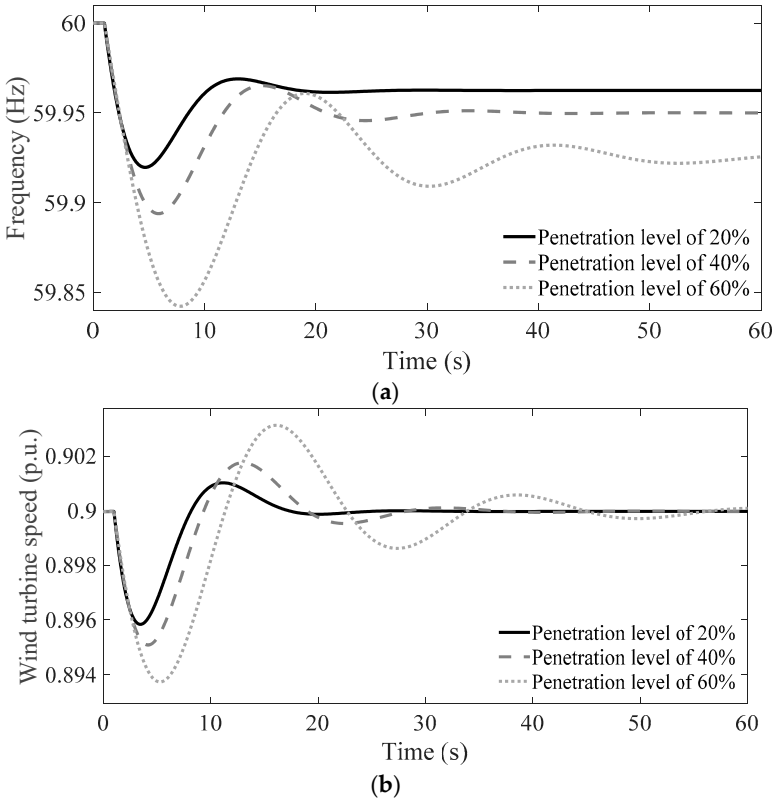

Figure 15. System dynamics considering different penetration levels of WG. (**a**) System frequency. (**b**) Wind turbine speed.

5. Conclusions

This work proposes a simplified model to assess the electromechanical dynamics of power systems with WG providing inertial response support. The proposed model allows the performance of simple and fast analyses that can provide an in-depth insight into the dynamics of the system frequency and equivalent WTG for different penetration levels of WG, wind speeds, virtual inertia values, control approaches, and load disturbances. The simplified model incorporates the antagonistic interaction between the MPPT and inertial controllers, which causes a relevant detrimental impact on the system frequency. The performed validation has shown that the proposed model, composed of four differential equations, describes the power system frequency dynamics with high accuracy.

As a second contribution, the work presents a comprehensive analysis of the main intrinsic and extrinsic aspects of WG that significantly affect the electromechanical dynamics

of power systems with WG providing inertial response support. The impact of wind speed, value of virtual inertia, WG penetration level, WTG control mode, and load variation magnitude on the system dynamics is comprehensively assessed. The results have shown that several aspects degrade the RoCoF, frequency nadir, and overall dynamic response of the system frequency.

The interaction between the MPPT and inertial controller couples the dynamics of the wind turbine speed and system frequency, degrading the frequency nadir and frequency oscillations. A significant increase in the virtual inertia results in a negligible improvement of the frequency nadir and a considerable increase in the amplitude of the frequency oscillations. Such detrimental behavior does not occur in conventional SGs, in which the increase in natural inertia significantly improves the frequency nadir. The higher the virtual inertia, the higher the amplitude of the frequency and wind turbine speed oscillations. The higher the load variation amplitude, the higher the amplitude of the frequency oscillations, which may result in a relevant second frequency dip. The increase in the wind speed, depending on the wind turbine aerodynamic characteristics, may slightly degrade the frequency dynamics, due to the increase in the nonlinearity of the mechanical power of the wind turbine. All addressed detrimental dynamics are mainly caused by the interactions of the MPPT and inertial controller and nonlinearities of the mechanical power curve of the wind turbine. In comparison with the MPPT control mode, the de-loaded control mode of WTGs with fixed power reference improves the frequency nadir and the frequency oscillations, due to the decoupling between the dynamics of the wind turbine speed and system frequency. The performed analyses have shown that inertial control is necessary but not sufficient to provide a suitable performance to power systems, since the increase in the penetration level of WG with inertial response support may significantly degrade the frequency nadir, steady-state frequency error, and frequency oscillations.

The performed analyses and the proposed model are useful to formulate new control approaches and to assist power system operators in the planning and operation of power systems. They also can be employed by engineers to design preventive and corrective actions to mitigate the negative detrimental interactions between the conventional MPPT and inertial controller, improving the electromechanical oscillations and frequency nadir, as well as extending the inertial response support of WG.

The incorporation of an equivalent photovoltaic generation in the simplified model is a direction of future prospective research, with emphasis on the impact of this kind of generation on the inertial response of power systems and the electromechanical dynamics of WG. Wind and photovoltaic generation without inertial response support will be incorporated in the equivalent model in such prospective research, considering a large set of operational scenarios in a Monte Carlo approach. The determination of complementary regression models from the proposed simplified model is also one of the future directions of this research.

Author Contributions: Conceptualization, B.A.B. and R.V.d.O.; methodology, B.A.B. and R.V.d.O.; software, B.A.B.; validation, B.A.B. and R.V.d.O.; formal analysis, B.A.B. and R.V.d.O.; investigation, B.A.B. and R.V.d.O.; resources, R.V.d.O.; data curation, B.A.B.; writing—original draft preparation, B.A.B. and R.V.d.O.; writing—review and editing, B.A.B. and R.V.d.O.; visualization, B.A.B.; supervision, R.V.d.O.; project administration, R.V.d.O.; funding acquisition, R.V.d.O. All authors have read and agreed to the published version of the manuscript.

Funding: The authors acknowledge UTFPR—Campus Pato Branco, FINEP, SETI, CNPq, and Fundação Araucária for scholarships and funding. This study was financed in part by the Coordenação de Aperfeiçoamento de Pessoal de Nível Superior—Brasil (CAPES)—Finance Code 001.

Conflicts of Interest: The authors declare no conflict of interest. The funders had no role in the design of the study; in the collection, analyses, or interpretation of data; in the writing of the manuscript; or in the decision to publish the results.

Appendix A. Description of the High-Order Model

The main components of the high-order model employed to validate the proposed model are described in this section. The SGs of the WTG and steam unit, control loops, wind turbine, inverter LCL filter, and electric load are the system main components. An upper bar is employed to describe the variables and parameters expressed in a per unit system (p.u.). The variables and parameters expressed in the international system of units do not have an upper bar.

The wind turbine mechanical power is described by [36,38]:

$$\overline{P}_{t,m} = \frac{1}{S_{sys,base}} \frac{1}{2} \rho_{ar} \pi r^2 C_p(\lambda, \beta) V_w^3, \tag{A1}$$

where V_w is the wind speed, β is the blade pitch angle, λ is the tip speed ratio, C_p is the power coefficient, r is the turbine radius, and ρ_{ar} is the air density. The power coefficient, as a function of λ and β, can be described by [36]:

$$C_p(\lambda, \beta) = 0.5176 \left(\frac{116}{\lambda_i} - 0.4\beta - 5 \right) e^{-\frac{21}{\lambda_i}} + 0.0068\lambda, \tag{A2}$$

where

$$\frac{1}{\lambda_i} = \frac{1}{\lambda + 0.08\beta} - \frac{0.035}{\beta^3 + 1}, \tag{A3}$$

and

$$\lambda = \frac{r\omega_t}{V_w}. \tag{A4}$$

The electrical dynamics inherent to the SGs of the steam unit and WTG are described by [39]:

$$\frac{d\, i_{ds}}{dt} = \left(-\overline{r}_s i_{ds} + \overline{L}_q i_{qs} \overline{\omega} + \frac{\overline{L}_{md}}{\omega_{base}} \frac{d\overline{i}_f}{dt} - \overline{v}_{ds} \right) \frac{\omega_{base}}{\overline{L}_d}, \tag{A5}$$

$$\frac{d\, i_{qs}}{dt} = \left(-\overline{r}_s i_{qs} - \overline{L}_d i_{ds} \overline{\omega} + \overline{L}_{md} i_f \overline{\omega} - \overline{v}_{qs} \right) \frac{\omega_{base}}{\overline{L}_q}, \tag{A6}$$

$$\frac{di_f}{dt} = \left(-\overline{r}_f i_f + \frac{\overline{L}_{md}}{\omega_{base}} \frac{di_{ds}}{dt} + \overline{v}_f \right) \frac{\omega_{base}}{\overline{L}_{fd}}, \tag{A7}$$

where $\overline{v}_{ds}$, $\overline{v}_{qs}$, and $\overline{v}_f$, are the stator voltages and field winding voltage, i_{ds}, i_{qs}, and i_f are the stator currents and field winding current, $\overline{L}_d$, $\overline{L}_q$, and $\overline{L}_{fd}$ are the stator inductances and field winding inductance, $\overline{r}_s$ and $\overline{r}_f$ are the stator resistance and field winding resistance, $\overline{L}_{md}$ is the mutual inductance, $\overline{\omega}$ is the angular speed of the generator [39]. The generator electromagnetic torque is described by [39]:

$$\overline{T}_e = \overline{L}_{md} i_f i_{qs} - \left(\overline{L}_d - \overline{L}_q \right) i_{ds} i_{qs} \Big). \tag{A8}$$

The wind turbine speed, which is equal to the SG speed, is described by:

$$J_t \omega_t \frac{d\omega_t}{dt} = P_{t,m} - P_{t,e}. \tag{A9}$$

In (A9), $P_{t,e}$ is the synchronous generator output power ($P_{t,e} = T_{t,e}\omega_t$, where $T_{t,e}$ is the electromagnetic torque similar to (A8)) and $P_{t,m}$ is the wind turbine mechanical power. The generator mechanical dynamics of the steam unit are described by [40]:

$$\frac{d\overline{\omega}_{sg}}{dt} = \frac{1}{2H_{sg}\overline{\omega}_{sg}} \left(\overline{P}_{sg,m} - \overline{P}_{sg,e} \right), \tag{A10}$$

$$\frac{d\delta}{dt} = (\overline{\omega}_{sg} - \overline{\omega}_n)\omega_{base}, \tag{A11}$$

In (A10) and (A11), $\overline{\omega}_{sg}$ is the generator angular speed corresponding to the steam unit, $\overline{P}_{sg,m}$ is the steam turbine mechanical power, $\overline{P}_{sg,e}$ is the SG output power ($\overline{P}_{sg,e} = \overline{T}_{sg,e}\overline{\omega}_{sg}$, where $\overline{T}_{sg,e}$ is the electromagnetic torque), δ is the generator rotor angle, $\overline{\omega}_n$ is the reference frame angular speed, and H_{sg} is the SG inertia constant.

The SG voltage regulators of the WTG and steam unit are standard proportional controllers. A first-order model (IEEE type-ST1 excitation system) is employed to model the generator excitation system.

The classical average model is employed to represent the WTG converters [27]. The control loops employed in the inverter can be found in [27]. The rectifier control loops employed in [19,25] are used in the WTG model. The classical model described in [41] is employed to represent the LCL filter of the WTG. A static ZIP load model is used to describe the system load [30].

References

1. Global Wind Energy Council (GWEC). Global Wind Report 2023, Technical Report. 2023. Available online: https://gwec.net/globalwindreport2023 (accessed on 20 June 2023).
2. Tielens, P.; Van Hertem, D. The relevance of inertia in power systems. *Renew. Sustain. Energy Rev.* **2016**, *55*, 999–1009. [CrossRef]
3. ENTSO-E. *Fast Frequency Reserve—Solution to the Nordic Inertia Challenge*; European Network of Transmission System Operators for Electricity Technical Report; 2019; pp. 1–22. Available online: https://www.fingrid.fi/en/news/news/2019/report-fast-frequency-reserve{-}{-}solution-to-the-nordic-inertia-challenge/ (accessed on 3 May 2023).
4. Xiong, L.; Li, P.; Wu, F.W.; Wang, J. Stability Enhancement of Power Systems with High DFIG-Wind Turbine Penetration via Virtual Inertia Planning. *IEEE Trans. Power Syst.* **2019**, *34*, 1352–1361. [CrossRef]
5. Ashouri-Zadeh, A.; Toulabi, M. Adaptive Virtual Inertia Controller for DFIGs Considering Nonlinear Aerodynamic Efficiency. *IEEE Trans. Sustain. Energy* **2021**, *12*, 1060–1067. [CrossRef]
6. Wang, J.; Xu, Y.; Wu, X.; Huang, J.; Zhang, X.; Yuan, H. Enhanced Inertial Response Capability of a Variable Wind Energy Conversion System. *Energies* **2021**, *14*, 8132. [CrossRef]
7. Gloe, A.; Jauch, C.; Craciun, B.; Winkelmann, J. Continuous provision of synthetic inertia with wind turbines: Implications for the wind turbine and for the grid. *IET Renew. Power Gener.* **2019**, *13*, 668–675. [CrossRef]
8. Qin, S.; Chang, Y.; Xie, Z.; Li, S. Improved Virtual Inertia of PMSG-Based Wind Turbines Based on Multi-Objective Model-Predictive Control. *Energies* **2021**, *14*, 3612. [CrossRef]
9. Mujcinagic, A.; Kusljugic, M.; Nukic, E. Wind Inertial Response Based on the Center of Inertia Frequency of a Control Area. *Energies* **2020**, *13*, 6177. [CrossRef]
10. Zhang, X.; Zhu, Z.; Fu, Y.; Li, L. Optimized virtual inertia of wind turbine for rotor angle stability in interconnected power systems. *Electr. Power Syst. Res.* **2020**, *180*, 106157. [CrossRef]
11. Liu, K.; Qu, Y.; Kim, H.M.; Song, H. Avoiding Frequency Second Dip in Power Unreserved Control during Wind Power Rotational Speed Recovery. *IEEE Trans. Power Syst.* **2018**, *33*, 3097–3106. [CrossRef]
12. Hwang, M.; Muljadi, E.; Jang, G.; Kang, Y.C. Disturbance-Adaptive Short-Term Frequency Support of a DFIG Associated with the Variable Gain Based on the ROCOF and Rotor Speed. *IEEE Trans. Power Syst.* **2017**, *32*, 1873–1881. [CrossRef]
13. Ravanji, M.H.; Canizares, C.A.; Parniani, M. Modeling and Control of Variable Speed Wind Tur-bine Generators for Frequency Regulation. *IEEE Trans. Sustain. Energy* **2020**, *11*, 916–927. [CrossRef]
14. Wu, Y.K.; Yang, W.H.; Hu, Y.L.; Dzung, P.Q. Frequency regulation at a wind farm using time-varying inertia and droop controls. *IEEE Trans. Ind. Appl.* **2019**, *55*, 213–224. [CrossRef]
15. Xi, J.; Geng, H.; Member, S.; Zou, X. Decoupling Scheme for Virtual Synchronous Generator Controlled Wind Farms. *J. Mod. Power Syst. Clean Energy* **2021**, *9*, 347–355. [CrossRef]
16. Xi, J.; Geng, H.; Ma, S.; Chi, Y.; Yang, G. Inertial response characteristics analysis and optimisation of PMSG-based VSG-controlled WECS. *IET Renew. Power Gener.* **2018**, *12*, 1741–1747. [CrossRef]
17. Tessaro, H.J.; De Oliveira, R.V. Impact assessment of virtual synchronous generator on the electromechanical dynamics of type 4 wind turbine generators. *IET Gener. Transm. Distrib.* **2019**, *13*, 5294–5304. [CrossRef]
18. Krpan, M.; Kuzle, I. Introducing low-order system frequency response modelling of a future power system with high penetration of wind power plants with frequency support capabilities. *IET Renew. Power Gener.* **2018**, *12*, 1453–1461. [CrossRef]
19. Yazdi, S.S.H.; Milimonfared, J.; Fathi, S.H.; Rouzbehi, K.; Rakhshani, E. Analytical modeling and inertia estimation of VSG-controlled Type 4 WTGs: Power system frequency response investigation. *Int. J. Electr. Power Energy Syst.* **2019**, *107*, 446–461. [CrossRef]
20. Bao, W.; Ding, L.; Liu, Z.; Zhu, G.; Kheshti, M.; Wu, Q.; Terzija, V. Analytically derived fixed termination time for stepwise inertial control of wind turbines—Part I: Analytical derivation. *Int. J. Electr. Power Energy Syst.* **2020**, *121*, 106120. [CrossRef]

21. Chu, Z.; Markovic, U.; Hug, G.; Teng, F. Towards optimal system scheduling with synthetic inertia provision from wind turbines. *IEEE Trans. Power Syst.* **2020**, *35*, 4056–4066. [CrossRef]
22. Bastiani, B.A.; de Oliveira, R.V. Adaptive MPPT control applied to virtual synchronous generator to extend the inertial response of type-4 wind turbine generators. *Sustain. Energy Grids Netw.* **2021**, *27*, 100504. [CrossRef]
23. Malekpour, M.; Zare, M.; Azizipanah-Abarghooee, R.; Terzija, V. Stochastic frequency constrained unit commitment incorporating virtual inertial response from variable speed wind turbines. *IET Gener. Transm. Distrib.* **2020**, *14*, 5193–5201. [CrossRef]
24. Wang, S.; Hu, J.; Yuan, X. Virtual Synchronous Control for Grid-Connected DFIG-Based Wind Turbines. *IEEE J. Emerg. Sel. Top. Power Electron.* **2015**, *3*, 932–944. [CrossRef]
25. Shang, L.; Hu, J.; Yuan, X.; Chi, Y. Understanding inertial response of variable-speed wind turbines by defined internal potential vector. *Energies* **2017**, *10*, 22. [CrossRef]
26. Tamrakar, U.; Shrestha, D.; Maharjan, M.; Bhattarai, B.; Hansen, T.; Tonkoski, R. Virtual Inertia: Current Trends and Future Directions. *Appl. Sci.* **2017**, *7*, 654. [CrossRef]
27. D'Arco, S.; Suul, J.A.; Fosso, O.B. Small-signal modeling and parametric sensitivity of a virtual synchronous machine in islanded operation. *Int. J. Electr. Power Energy Syst.* **2015**, *72*, 3–15. [CrossRef]
28. Muftau, B.; Fazeli, M.; Egwebe, A. Stability analysis of a PMSG based Virtual Synchronous Machine. *Electr. Power Syst. Res.* **2020**, *180*, 106170. [CrossRef]
29. Rodriguez Medina, D.; Rappold, E.; Sanchez, O.; Luo, X.; Rivera Rodriguez, S.R.; Wu, D.; Jiang, J.N. Fast Assessment of Frequency Response of Cold Load Pickup in Power System Restoration. *IEEE Trans. Power Syst.* **2016**, *31*, 3249–3256. [CrossRef]
30. Kundur, P. *Power System Stability And Control*; McGraw-Hill: New York, NY, USA, 1994.
31. Lin, S.; Yao, W.; Zhao, Y.; Shi, Z.; Peng, L.; Cheng, Y.; Ai, X.; Wen, J. Vector-variable based modeling method for large-scale wind farm considering collector system dynamics. *Int. J. Electr. Power Energy Syst.* **2023**, *149*, 109016. [CrossRef]
32. Zou, J.; Peng, C.; Yan, Y.; Zheng, H.; Li, Y. A survey of dynamic equivalent modeling for wind farm. *Renew. Sustain. Energy Rev.* **2014**, *40*, 956–963. [CrossRef]
33. Wang, P.; Zhang, Z.; Huang, Q.; Wang, N.; Zhang, X.; Lee, W.J. Improved wind farm aggregated modeling method for large-scale power system stability studies. *IEEE Trans. Power Syst.* **2018**, *33*, 6332–6342. [CrossRef]
34. Baimel, D.; Belikov, J.; Guerrero, J.M.; Levron, Y. Dynamic Modeling of Networks, Microgrids, and Renewable Sources in the dq0 Reference Frame: A Survey. *IEEE Access* **2017**, *5*, 21323–21335. [CrossRef]
35. Van De Vyver, J.; De Kooning, J.D.M.; Meersman, B.; Vandevelde, L.; Vandoorn, T.L. Droop Control as an Alternative Inertial Response Strategy for the Synthetic Inertia on Wind Turbines. *IEEE Trans. Power Syst.* **2016**, *31*, 1129–1138. [CrossRef]
36. Boyle, J.; Littler, T.; Foley, A. Review of frequency stability services for grid balancing with wind generation. *J. Eng.* **2018**, *15*, 1061–1065. [CrossRef]
37. Huang, L.; Xin, H.; Zhang, L.; Wang, Z.; Wu, K.; Wang, H. Synchronization and Frequency Regulation of DFIG-based Wind Turbine Generators with Synchronized Control. *IEEE Trans. Energy Convers.* **2017**, *32*, 1251–1262. [CrossRef]
38. Nguyen, D.; Fujita, G. Analysis of sensorless MPPT method for hybrid PV-Wind system using DFIG Wind Turbines. Sustain. *Energy Grids Netw.* **2016**, *5*, 50–57. [CrossRef]
39. Anaya-Lara, O.; Jenkins, N.; Ekanayake, J.; Cartwright, P.; Hughes, M. *Wind Energy Generation: Modelling and Control*; John Wiley & Sons: Hoboken, NJ, USA, 2009.
40. Das, D.; Aditya, S.K.; Kothari, D.P. Dynamics of diesel and wind turbine generators on an isolated power system. *Int. J. Electr. Power Energy Syst.* **1999**, *21*, 183–189. [CrossRef]
41. Pogaku, N.; Prodanovic, M.; Green, T.C. Modeling, Analysis and Testing of Autonomous Operation of an Inverter-Based Microgrid. *IEEE Trans. Power Electron.* **2007**, *22*, 613–625. [CrossRef]